Eur. Phys. J. E (2016) **39**: 33
DOI 10.1140/epje/i2016-16033-6

THE EUROPEAN PHYSICAL JOURNAL E

Regular Article

Thermophysical effects of water driven copper nanoparticles on MHD axisymmetric permeable shrinking sheet: Dual-nature study

Rizwan Ul Haq[1,a], D. Rajotia[2], and N.F.M. Noor[3]

[1] Department of Mathematics, Capital University of Science and Technology, Islamabad, Pakistan
[2] Department of Mathematics, University of Rajasthan, Jaipur, 302004 India
[3] Institute of Mathematical Sciences, Faculty of Science, University of Malaya, 50603 Kuala Lumpur, Malaysia

Received 1 October 2015 and Received in final form 30 December 2015
Published online: 24 March 2016 –

Abstract. The present study is dedicated to analyze the dual-nature solutions of the axisymmetric flow of a magneto-hydrodynamics (MHD) nanofluid over a permeable shrinking sheet. In those phenomena where the fluid flow is due to the shrinking surface, some reverse behaviors of the flow arise because of vorticity effects. Despite of heat transfer analysis, the main purpose of the present study is to attain the solutions of the complex nature problem that appear in reverse flow phenomena. Thermophysical properties of both base fluid (water) and nanoparticles (copper) are also taken into account. By means of similarity transformation, partial differential equations are converted into a system of coupled nonlinear ordinary differential equations and then solved via the Runge-Kutta method. These results are divided separately into two cases: the first one is the unidirectional shrinking along the surface ($m = 1$) and the other one is for axisymmetric shrinking phenomena ($m = 2$). To enhance the thermal conductivity of base fluid, nanoparticle volume fractions ($0 \leq \phi \leq 0.2$) are incorporated within the base fluid. The numerical investigation explores the condition of existence, non-existence and the duality of similarity solution depends upon the range of suction parameter (S) and Hartmann number (M). The reduced skin friction coefficient and local Nusselt number are plotted to analyze the fluid flow and heat transfer at the surface of the shrinking sheet. Streamlines and isotherms are also plotted against the engineering control parameters to analyze the flow behavior and heat transfer within the whole domain. Throughout this analysis it is found that both nanoparticle volume fraction and Hartmann number are increasing functions of both skin friction coefficient and Nusselt number.

1 Introduction

There is an extensive range of industrial process in which enhancement and transfer of heat energy is most commonly used at any industrial level. In fact, it is a major task when heat must be removed, added, or when the transfer of process stream from one to another place has become an industrial necessity. The improvement in the progress of the high thermal system to enhance its thermal conductivity and heat transfer rate has become a common issue. A considerable amount of research has been accomplished to achieve better heat transfer performance for industrial applications. So, according to all these theories and research, a better heat transfer process requires, advanced technologies for heat transfer. There are several methods to improve heat transfer efficiency. One of the ways is by increasing the thermal conductivity of the working fluid, since the heat transfer of the base fluids such as water, engine oil and ethylene glycol has comparatively low thermal conductivities as compared to the thermal conductivity of solids. So those solids with high thermal conductivity can be used to enhance the thermal conductivity of the based fluid by incorporating the small tiny particles to that fluid. Thus, such kind of tiny solid particle is known as "nanoparticle" which ranges from 1–100 nm in diameter and its structure varies according to shape and size. The homogenous mixture of the base fluid and nanoparticle is known as "nanofluid". The main vision of incorporating the nanoparticles within the base fluid to enhance thermal conductivity was introduced by Choi [1] in 1995.

Beside the concept of nanofluid, it was found that heat transfer could be excellent but at the rate of a high cost of pumping power. Initially, Choi concluded that the effect of thermal conductivity of a nanofluid is much better than a high cost of pumping power for heat

[a] e-mail: ideal_riz@hotmail.com, dr.haq@cust.edu.pk

transfer efficiency. Therefore, incorporations of nanoparticles within the base fluid are not only beneficial for a high thermal system but somehow it is economically cheaper. Nanoparticles are made from different materials, such as metal nitrides (AlN, SiN), carbide ceramics (Sic, Tic), oxide ceramics (Al_2O_3, CuO), metals (Cu, Ag, Au), carbons in various forms (*e.g.*, diamond, graphite, carbon nanotubes, fullerene) and functionalized nanoparticles. Lixin Cheng [2] presented the brief concept of nanofluid with heat transfer and the influence of thermal conductivity of different materials like carbon, metallic solids, non-metallic solids, metallic liquids and many others. Recently, in 2005, Buongiorno [3] proposed seven foremost slip mechanisms, namely: inertia, Brownian diffusion, thermophoresis, diffusionphoresis, Magnus effect, fluid drainage and gravity settling. His major concern was to complete the transport model of nanofluids.

Recently, fluid flows over a horizontally or a vertically stretching/shrinking sheet surface attracted the attention of many researchers due to their wide range of applications at the industrial level, such as: shrinking wrapping, bundle wrapping, hot rolling, extrusion of sheet material, wire rolling, and glass fiber. The fluid flow over a shrinking surface towards a slot is quite different from the stretching case. The physical cause behind the shrinking surface is that the vorticity produced due to the shrinking sheet is not confined within the boundary layer and consequently, a situation appears where some other external forces are to be imposed. In order to confine the vorticity within the boundary layer, some external forces are imposed in the form of suction/injection at the sheet presented by Miklavcic and Wang [4] or stagnation added to the main flow by Wang [5]. Later on several researchers studied the boundary layer flows over a shrinking surface under different physical conditions [6–9].

Nield and Kuznetsov [10] analyzed the Cheng-Minkowycz problem for natural convection flow past a vertical plate in a porous medium saturated by a nanofluid. In the view of the existing literature, Nield and Kuznetsov extended their own work for double-diffusive natural convective boundary layer flow of a nanofluid [11]. Initially, Khan and Pop [12] presented the idea of a nanofuid flow past a stretching sheet where they concluded the significant contributions of Brownian motion and thermophoresis effects for heat transfer and nanoparticle concentration. The unsteady boundary layer flow and heat transfer of nanofluid over a permeable stretching/shrinking sheet was investigated by Bachok *et al.* [13] and they have found that dual solutions exist for shrinking sheet. In another paper, Rohni *et al.* [14] discussed the effects of the wall mass suction $S(>0)$, the unsteadiness $A(<0)$ and the nanofluid parameters on the flow, heat transfer and concentration characteristics. They found that non-unique solutions exist for certain chosen parameters, and the flow and heat transfer are significantly influenced by these parameters. More recently the effects of slip and heat generation/absorption on MHD boundary layer stagnation point flow and heat transfer of nanofluid over a stretching/shrinking surface were analyzed by Nandy and Mahapatra [15]. In the last few years, studies related to nanofluid attained considerable attention because of its higher thermal conductivity for both Newtonian and non-Newtonian fluids [16–20].

The primary objective of the present study is to analyze the flow and heat transfer of nanofluid along a three-dimensional axisymmetric shrinking sheet. We further consider the porosity sheet to reduce the vorticity effects. This nanofluid mixture contains water and copper nanoparticles. A model of the problem is proposed along two lateral directions according to the values of m. The mathematical model is constructed in the form of partial differential equations which then reduced to ordinary differential equations through similarity transformation. Throughout the analysis, we use the thermophysical properties of both base fluid and nanoparticle. Dual-nature solutions are constructed for velocity, temperature, reduced skin friction coefficient and reduced Nusselt number against each physical parameter. Conclusions have been drawn based on the whole analysis outcomes.

2 Mathematical analysis

Consider three-dimensional MHD flow of water functional copper (Cu) nanoparticles due to a shrinking sheet along the axisymmetric direction. The strength of the magnetic field B_0 is applied normal to the surface. The induced magnetic field is negligible with assumption of small magnetic Reynolds number. According to the three-dimensional frame of reference, the velocity components (u, v, w) are adjusted along the (x, y, z) directions, respectively (see fig. 1). Fluid is flowing due to the shrinking of the surface along both directions and we further consider the suction/injection force at the surface to reduce the vorticity effects. Moreover, the condition of uniform heat flux [21, 22] is assumed at the surface. The basic governing equations of the problem given by Miklavcic and Wang [4] are

$$\frac{\partial u}{\partial x}+\frac{\partial v}{\partial y}+\frac{\partial w}{\partial z}=0, \tag{1}$$

$$u\frac{\partial u}{\partial x}+v\frac{\partial u}{\partial y}+w\frac{\partial u}{\partial z}=-\frac{1}{\rho_{\rm nf}}\frac{\partial p}{\partial x}+\frac{\mu_{\rm nf}}{\rho_{\rm nf}}\left(\frac{\partial^2 u}{\partial x^2}+\frac{\partial^2 u}{\partial y^2}+\frac{\partial^2 u}{\partial z^2}\right)-\frac{\sigma B_0^2}{\rho_{\rm nf}}u, \tag{2}$$

$$u\frac{\partial v}{\partial x}+v\frac{\partial v}{\partial y}+w\frac{\partial v}{\partial z}=-\frac{1}{\rho_{\rm nf}}\frac{\partial p}{\partial y}+\frac{\mu_{\rm nf}}{\rho_{\rm nf}}\left(\frac{\partial^2 v}{\partial x^2}+\frac{\partial^2 v}{\partial y^2}+\frac{\partial^2 v}{\partial z^2}\right)-\frac{\sigma B_0^2}{\rho_{\rm nf}}v, \tag{3}$$

$$u\frac{\partial w}{\partial x}+v\frac{\partial w}{\partial y}+w\frac{\partial w}{\partial z}=-\frac{1}{\rho_{\rm nf}}\frac{\partial p}{\partial z}+\frac{\mu_{\rm nf}}{\rho_{\rm nf}}\left(\frac{\partial^2 w}{\partial x^2}+\frac{\partial^2 w}{\partial y^2}+\frac{\partial^2 w}{\partial z^2}\right), \tag{4}$$

$$u\frac{\partial T}{\partial x}+v\frac{\partial T}{\partial y}+w\frac{\partial T}{\partial z}=\alpha_{\rm nf}\left(\frac{\partial^2 T}{\partial x^2}+\frac{\partial^2 T}{\partial y^2}+\frac{\partial^2 T}{\partial z^2}\right), \tag{5}$$

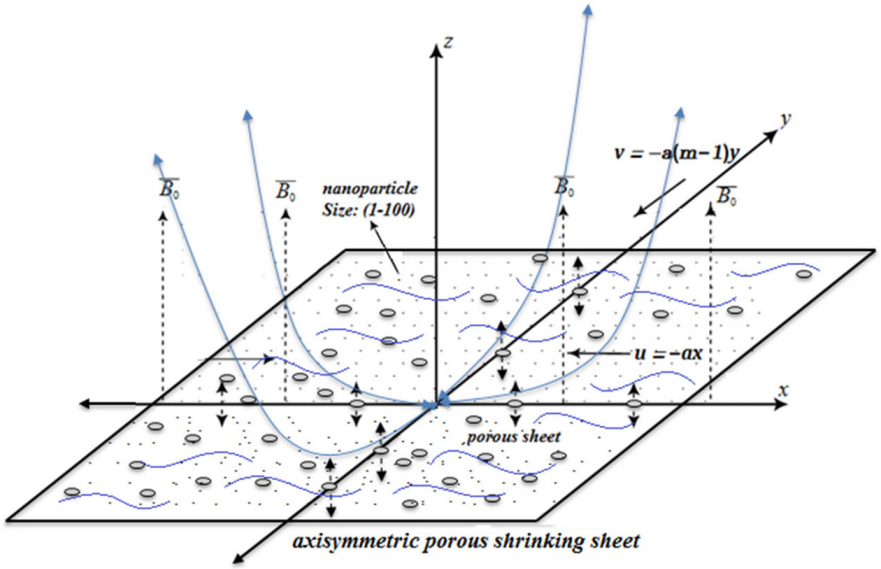

Fig. 1. Geometry of the problem.

where p is the pressure, T is the temperature of the nanofluid, $\alpha_{\rm nf}$ is the thermal diffusivity of nanofluid, $\rho_{\rm nf}$ is the density of nanofluid, $\nu_{\rm nf}$ is the kinematic viscosity of the nanofluid and $\mu_{\rm nf}$ is the dynamic viscosity of the nanofluid which are defined as

$$\left.\begin{aligned}
&\mu_{\rm nf}=\frac{\mu_f}{(1-\phi)^{2.5}}\,, \quad \nu_{\rm nf}=\frac{\mu_{\rm nf}}{\rho_{\rm nf}}\,, \quad \rho_{\rm nf}=(1-\phi)\rho_f+\phi(\rho)_s,\\
&\alpha_{\rm nf}=\frac{k_{\rm nf}}{(\rho C_p)_{\rm nf}}\,, \quad (\rho C_p)_{\rm nf}=(1-\phi)(\rho C_p)_f+\phi(\rho C_p)_s,\\
&\frac{k_{\rm nf}}{k_f}=\frac{(k_s+2k_f)-2\phi(k_f-k_s)}{(k_s+2k_f)+\phi(k_f-k_s)}\,.
\end{aligned}\right\} \tag{6}$$

In the above expressions, ϕ is the nanoparticle volume fraction, $(\rho C_p)_{\rm nf}$ is the effective heat capacity of nanoparticle, $k_{\rm nf}$ is the thermal conductivity of nanofluid, k_f and k_s are the thermal conductivities of the base fluid and nanoparticles respectively, ρ_f and ρ_s are the densities of the base fluid and nanoparticles, respectively. Hence the shrinking velocity and temperature at the wall of the present model are defined as

$$\begin{aligned}
&u=-U_{wx}=-ax, \qquad v=-V_{wy}=-a(m-1)y,\\
&w=-W, \qquad \frac{\partial T}{\partial z}=-\frac{q_w}{k_f}\,, \qquad C=C_w \quad \text{at } z=0,\\
&u\to 0, \qquad v\to 0, \qquad T\to T_\infty \quad \text{as } z\to\infty,
\end{aligned} \tag{7}$$

where $a>0$ is the shrinking constant with dimension (1/time), $W>0$ is the suction velocity and q_w is the surface heat flux. In the present study it is important to note that there are two cases which are defined as $m=1$ when the sheet is shrinking along in the x-direction and for $m=2$ when the sheet is shrinking along both x and y directions (axisymmetrically). The following similarity transformations are introduced:

$$\begin{aligned}
&\eta=\sqrt{\frac{a}{\nu_f}}z, \qquad u=axf'(\eta), \qquad v=a(m-1)yf'(\eta),\\
&w=-\sqrt{a\nu_f}mf(\eta), \qquad \theta(\eta)=\frac{k_f(T-T_\infty)}{q_w}\sqrt{\frac{a}{\nu_f}}\,.
\end{aligned} \tag{8}$$

From eqs. (1)–(5), eq. (1) is identically satisfied while eq. (4) can be integrated as

$$\frac{p}{\rho_f}=\frac{\mu_{\rm nf}}{\rho_{\rm nf}}\frac{\partial w}{\partial z}-\frac{w^2}{2}+\text{constant}. \tag{9}$$

By means of eq. (8), the predefined eqs. (2)–(4) take the following form:

$$\begin{aligned}
&\frac{1}{(1-\phi)^{2.5}\left(1-\phi+\phi\dfrac{\rho_s}{\rho_f}\right)}f'''+mff''-f'^2\\
&-\frac{M^2f'}{\left(1-\phi+\phi\dfrac{\rho_s}{\rho_f}\right)}=0,
\end{aligned} \tag{10}$$

$$\frac{1}{\rm Pr}\frac{(k_{\rm nf}/k_f)}{\left(1-\phi+\phi\dfrac{(\rho)_s(C_p)_s}{(\rho)_f(C_p)_f}\right)}\theta''+mf\theta'=0. \tag{11}$$

Consequently, the corresponding boundary conditions defined in eq. (7) will take the following form:

$$\begin{aligned}
&f(0)=S, \qquad f'(0)=-1, \qquad \theta'(0)=-\frac{1}{k_{\rm nf}/k_f}\,,\\
&f'(\eta)=0, \qquad \theta(\eta)=0 \quad \text{as } \eta\to\infty.
\end{aligned} \tag{12}$$

In the last three above equations, $M^2=\frac{\sigma B_o^2}{\rho_f a}$ is the Hartmann number, $S=W/m\sqrt{a\nu_f}$ is the suction/injection

parameter, $\mathrm{Pr} = \nu_f/\alpha$ is the Prandtl number. The expressions for local skin friction coefficients C_{fx} and C_{fy} along the x- and y-direction are respectively defined as

$$C_{fx} = \frac{\tau_{wx}}{\rho_f U_{wx}^2} = \frac{\mu_{\mathrm{nf}}\left(\frac{\partial u}{\partial z}\right)_{z=0}}{\rho_f U_{wx}^2} = \frac{1}{\sqrt{\mathrm{Re}_x}(1-\phi)^{2.5}} f''(0),$$
$$C_{fy} = \frac{\tau_{wy}}{\rho_f V_{wy}^2}\frac{\mu_{\mathrm{nf}}\left(\frac{\partial v}{\partial z}\right)_{z=0}}{\rho_f V_{wy}^2} = \frac{1}{\sqrt{\mathrm{Re}_x}(1-\phi)^{2.5}} f''(0), \tag{13}$$

where the dimensionless form of the local Nusselt number Nu_x is defined as

$$Nu_x = \frac{x q_w}{k_f\,(T_w - T_\infty)} = \frac{x\left(-k\frac{\partial T}{\partial y}\right)_{y=0}}{k_f\,(T_w - T_\infty)} = -\sqrt{\mathrm{Re}_x}\frac{k_{\mathrm{nf}}}{k_f}\frac{1}{\theta(0)}. \tag{14}$$

In eqs. (13) and (14) above, $\mathrm{Re}_x = xU_{wx}/\nu$ and $\mathrm{Re}_y = yV_{wy}/\nu$ are local Reynolds number along the x- and y-directions, respectively.

3 Methodology

The dimensionless form of the above system of differential equations defined in eqs. (10)–(11) along with the boundary conditions defined in (12) are solved numerically with the help of the Runge-Kutta method in a computational software MATLAB. To solve the boundary value problem, we first convert this system into the initial value problem with the help of the shooting technique. The following system is established:

$$\left.\begin{aligned} x_1 &= f,\\ x_2 &= f',\\ x_3 &= x_2' = f'',\\ x_4 &= x_3' = f''' = -(1-\phi)^{2.5}(1-\phi+\phi\rho_s/\rho_f)\\ &\quad\times\left(m x_1 x_3 - x_2^2 - M^2 x_2/\left(1-\phi+\phi\rho_s/\rho_f\right)\right), \end{aligned}\right\} \tag{15}$$

$$\left.\begin{aligned} y_1 &= \theta,\\ y_2 &= \theta',\\ y_3 &= y_2' = \theta'' = -\frac{\mathrm{Pr}\,(1-\phi+\phi(\rho C_p)_s/(\rho C_p)_f)}{k_{\mathrm{nf}}/k_f} m x_1 y_2. \end{aligned}\right\} \tag{16}$$

The corresponding initial conditions take the following form:

$$x_1(0) = S, \qquad x_2(0) = -1, \qquad y_2(0) = -\frac{1}{k_{\mathrm{nf}}/k_f}. \tag{17}$$

In order to integrate eqs. (15) and (16) with respect to the initial condition (17), one must use the values $x_3(0) = f''(0)$ and $y_2(0) = \theta'(0)$ but no such values are given within the boundary conditions. The appropriate guessed values for $f''(0)$ and $\theta'(0)$ are chosen and then integration is implemented. Then the calculated values for $f'(\eta)$ and $\theta(\eta)$ at $\eta = 12$ (say) are associated with the given boundary conditions as $f'(\eta) = 0$ and $\theta(\eta) = 0$ while the estimated values of $f''(0)$ and $\theta'(0)$ are adjusted to give a better approximation for the solution. We take the series of values for $f''(0)$ and $\theta'(0)$ and then further apply the fourth-order classical Runge-Kutta method with step size $\Delta\eta = 0.001$. The above procedure is repeated until we get the asymptotically converged results within a tolerance level of 10^{-7}.

Table 1. Thermophysical properties of base fluid and nanoparticle.

Physical properties	Fluid phase (water)	Cu
C_p (J/kg K)	4179	385
ρ (kg/m^3)	997.1	8933
k (W/mk)	0.613	400
$\beta \times 10^7$ (m^2/s)	1.47	1166.1

4 Results analysis and discussion

4.1 Numerical tables

One of the most significant objectives that appear in this article is to use the thermophysical values of emerging parameters. For this we used some particular values which are collected through some experimental data as mentioned in table 1. Before producing the graphical results, it is important to analyze the existence of a solution. For this purpose, we have tabulated the range for solution existence in table 2. Through table 2, the range of S is defined for both cases; unidirectional shrinking along the x-direction ($m = 1$) and secondly for the axisymmetric shrinking case ($m = 2$).

To validate our results with the existing literature, comparison is made with the results produced by Noor *et al.* [23]. In table 3 it is found that results produced via the Runge-Kutta method is in good agreement with the Adomain decomposition method.

4.2 Analysis of skin friction coefficient and local Nusselt number

In order to discuss the fluid flow behavior over the shrinking sheet, results are plotted for skin friction $f''(0)/(1-\phi)^{2.5}$ against the emerging parameters such as the suction/injection parameter S, the Hartmann number M and the nanoparticle volume fraction ϕ. All these results are constructed for $m = 1$ when the sheet is shrinking along the x-direction and $m = 2$ when the sheet shrinks axisymmetrically. Figure 2(a) demonstrates the influence of the suction parameter S and Hartmann number M on

Table 2. Range of S for existence of dual solutions with several values of M.

M^2	ϕ	Existence of dual solution		Non-existence of solution	
		$m=1$	$m=2$	$m=1$	$m=2$
0	0	$S \geq 2.0000$	$S \geq 1.3117$	$S < 2.0000$	$S < 1.3117$
0	0.05	$S \geq 1.8036$	$S \geq 1.1830$	$S < 1.8036$	$S < 1.1830$
0	0.1	$S \geq 1.7025$	$S \geq 1.1166$	$S < 1.7025$	$S < 1.1166$
0	0.15	$S \geq 1.6545$	$S \geq 1.0852$	$S < 1.6545$	$S < 1.0852$
0	0.2	$S \geq 1.6420$	$S \geq 1.0770$	$S < 1.6420$	$S < 1.0770$
0.1	0	$S \geq 1.8973$	$S \geq 1.2685$	$S < 1.8973$	$S < 1.2685$
0.2	0	$S \geq 1.7888$	$S \geq 1.2232$	$S < 1.7888$	$S < 1.2232$
0.3	0	$S \geq 1.6733$	$S \geq 1.1753$	$S < 1.6733$	$S < 1.1753$
0.4	0	$S \geq 1.5419$	$S \geq 1.1244$	$S < 1.5419$	$S < 1.1244$
0.5	0	$S \geq 1.4915$	$S \geq 1.1070$	$S < 1.4915$	$S < 1.1070$
0.2	0.05	$S \geq 1.6696$	$S \geq 1.1266$	$S < 1.6696$	$S < 1.1266$
0.2	0.1	$S \geq 1.6049$	$S \geq 1.0756$	$S < 1.6049$	$S < 1.0756$
0.2	0.2	$S \geq 1.5774$	$S \geq 1.0497$	$S < 1.5774$	$S < 1.0497$
0.4	0.05	$S \geq 1.5239$	$S \geq 1.0660$	$S < 1.5239$	$S < 1.0660$
0.4	0.1	$S \geq 1.5010$	$S \geq 1.0330$	$S < 1.5010$	$S < 1.0330$
0.4	0.2	$S \geq 1.4995$	$S \geq 1.0215$	$S < 1.4995$	$S < 1.0215$

Table 3. Comparison table for numerical values of $f''(0)$ in the absence of the nanoparticle volume fraction ($\phi = 0$) when $S = 1$ and $M = 2$.

Padé approximant	$m=1$		$m=2$	
	ADM	R-K method	ADM	R-K method
[5/5]	2.30273 ref. [23]	2.30277	1.33605 ref. [23]	2.98131
[10/10]	2.30278 ref. [23]	2.30277	2.98131 ref. [23]	2.98131
[15/15]	2.30278 ref. [23]	2.30277	2.98131 ref. [23]	2.98131
[20/20]	2.30278 ref. [23]	2.30277	2.98131 ref. [23]	2.98131

the reduced skin friction coefficient $f''(0)/(1-\phi)^{2.5}$ for $m = 1$. It is observed that for $1.4 \leq S \leq 3$, there is a dual-nature solution for skin friction coefficient when $M = 0$, 0.2 and 0.4. Critical values are also determined for the domain S, where the solution obtained for skin friction is divided into two parts; lower and upper branches. It is further observed that for the upper branch solution, an increase in both suction parameter S and MHD parameter M caused an increase in the skin friction coefficient; however, the results are quite opposite for the lower branch. Physically, this phenomenon occurs in the appearance of the Lorentz force which resists the motion of fluid particle. In fig. 2(b), the analysis performed for the axisymmetric shrinking case ($m = 2$) is quite similar when it is compared with fig. 2(a) for $m = 1$. Furthermore, it can also be determined through fig. 2(b), with an increase of the S skin friction will rise for both upper and lower branch solutions. Figure 3 demonstrates the variation of the skin friction coefficient $f''(0)/(1-\phi)^{2.5}$ with respect to the suction/injection parameter S and nanoparticle volume fraction ϕ for both unidirectional and axisymmetric flow. Again from analysis, the dual-nature solutions are plotted against the various values of the physical parameters. Through this analysis, it is found that skin friction is a decreasing function of nanoparticle volume fraction in the stable part of the solution. The behaviors captured by the graphs are applicable under the analysis of higher density of mixture after saturating the nanoparticle volume fraction ϕ in the base fluid (water). So we can observe in fig. 3(a) that water ($\phi = 0$) has a lower skin friction as compared to the nanofluid ($\phi = 0.05, 0.1$). Results provided in fig. 3(b) show the similar behaviors as shown in

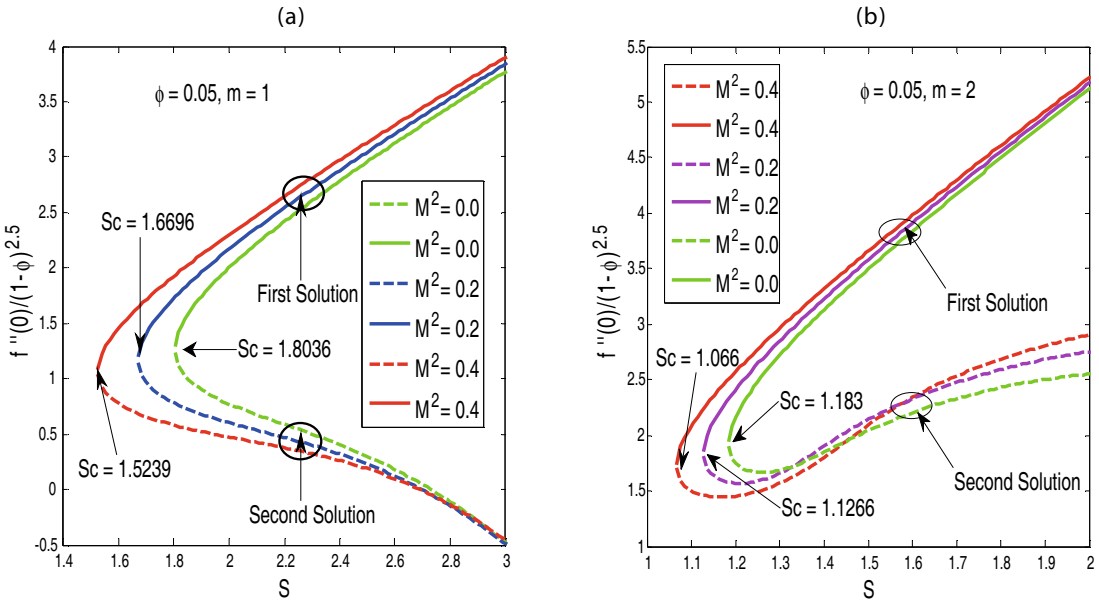

Fig. 2. (a): Variation of reduced skin friction for various values of M and S when $m = 1$. (b): Variation of reduced skin friction for various values of M and S when $m = 2$.

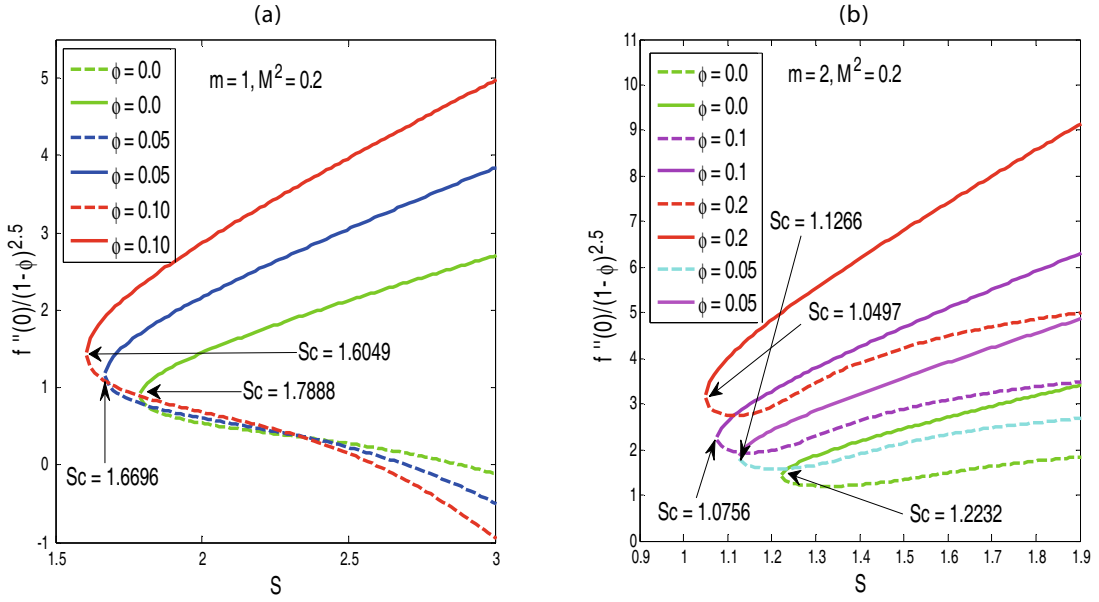

Fig. 3. (a): Variation of reduced skin friction for various values of ϕ and S when $m = 1$. (b): Variation of reduced skin friction for various values of ϕ and S when $m = 2$.

fig. 3(a). However for $m = 2$, the variation in the skin friction is more dominant with respect to various values of the nanoparticle volume fraction ϕ (see fig. 3(b)).

To examine the heat transfer rate at the surface of the shrinking sheet, results are plotted in fig. 4 and fig. 5 for a reduced Nusselt number $k_{\rm nf}/k_f\theta(0)$ against the Hartmann number M, suction/injection parameter S and nanoparticle volume fraction ϕ. It can be analyzed that both lower and upper branch solutions of the reduced Nusselt number $k_{\rm nf}/k_f\theta(0)$ provide the opposite trend of results with respect to the upper and lower branches of the solution. One can see that in the lower region of the solution, there is an increase in the absolute reduced Nusselt number with respect to an increase in the MHD parameter M (see fig. 4(a)). However, the trend of the plots in the upper region of the solution is quite opposite and gives a decreasing behavior for increasing values of the MHD parameter. Although the variation in the reduced Nusselt number is not dominant in the onsets of fig. 4(a) and (b), the results are varying with respect to the variation of each physical parameter as S increases. Figure 5(a) and (b) display the simultaneous effects of the suction/injection

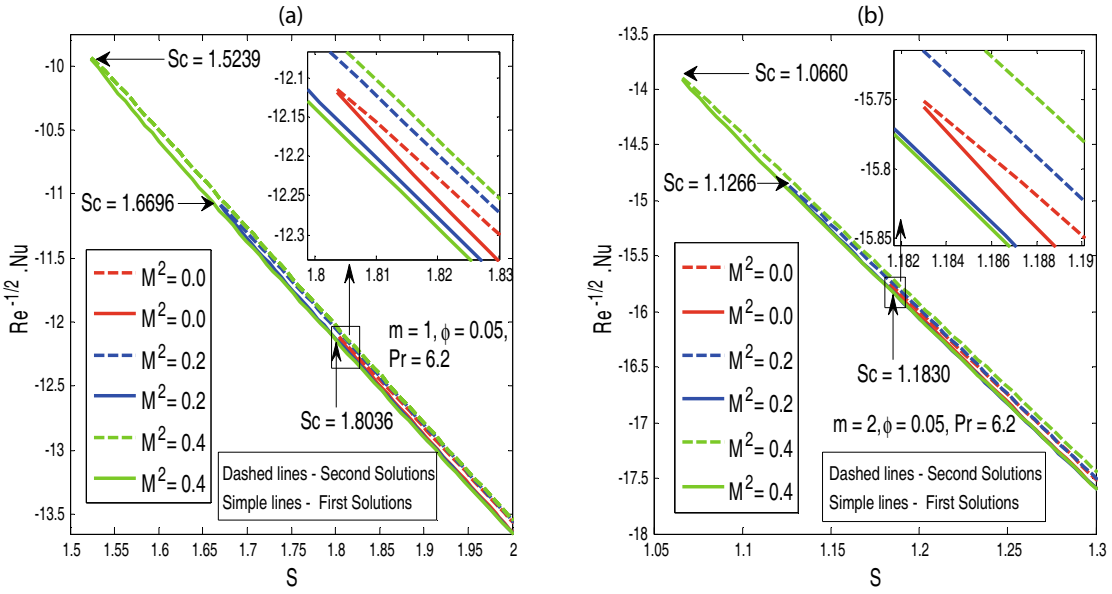

Fig. 4. (a): Variation of reduced Nusselt number for various values of M and S when $m = 1$. (b): Variation of reduced Nusselt number for various values of M and S when $m = 2$.

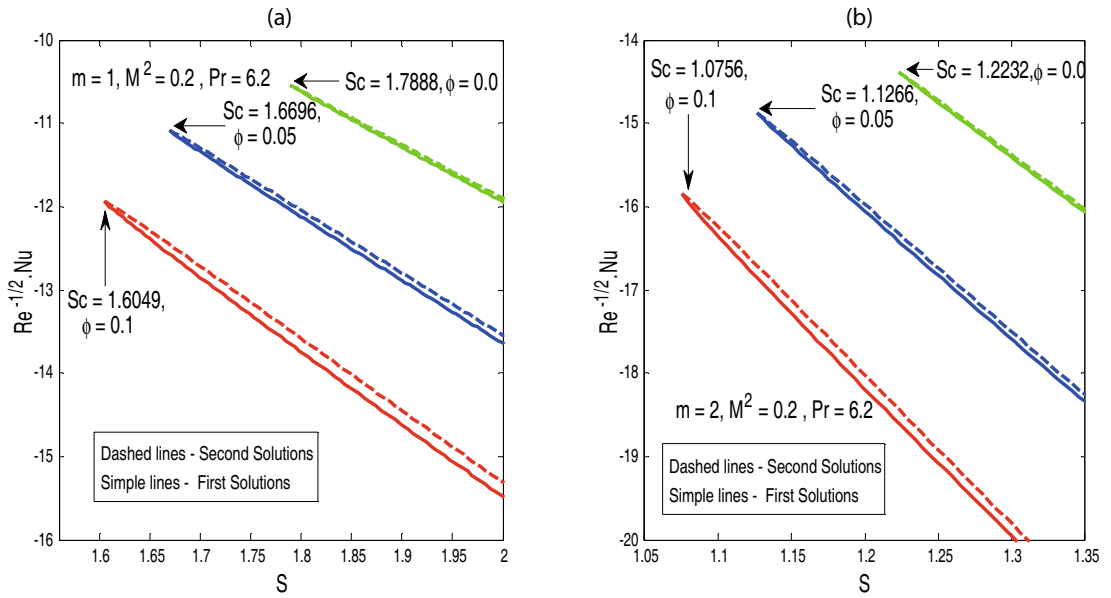

Fig. 5. (a): Variation of reduced Nusselt number for various values of ϕ and S when $m = 1$. (b): Variation of reduced Nusselt number for various values of ϕ and S when $m = 2$.

parameter S and the nanoparticle volume fraction ϕ on the reduced Nusselt number $k_{\rm nf}/k_f\theta(0)$. It can be observed that, against the suction/injection parameter S, dual-nature solutions are attained for the reduced Nusselt number $k_{\rm nf}/k_f\theta(0)$ for each value of the nanoparticle volume fraction ϕ. If we observe the absolute values of the reduced Nusselt number, it is found that the base fluid ($\phi = 0$) gives a lower heat transfer rate at the surface as compared to the nanofluid when $\phi = 0.05$ and $\phi = 0.1$, respectively. Through figs. 4 and 5, it can be ascertained that for both values for m (= 1 and 2), the absolute reduced Nusselt number is increasing with the increasing values of S.

4.3 Analysis of velocity and temperature profile

Figures 6–10 are plotted for velocity $f'(\eta)$ and temperature distribution $\theta(\eta)$ against the dimensionless parameters such as the suction/injection parameter S, the Hartmann number M and the nanoparticle volume fraction ϕ. All these results are plotted for both values of m (= 1, 2).

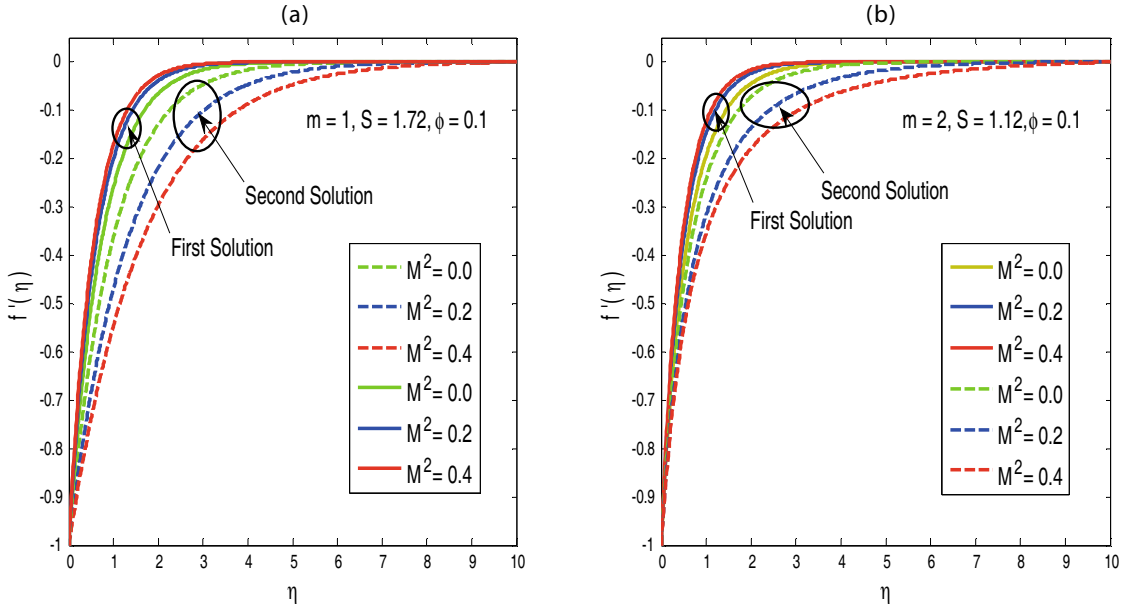

Fig. 6. (a): Variation of velocity profile $f'(\eta)$ for various values of M for $m = 1$. (b): Variation of velocity profile $f'(\eta)$ for various values of M when $m = 2$.

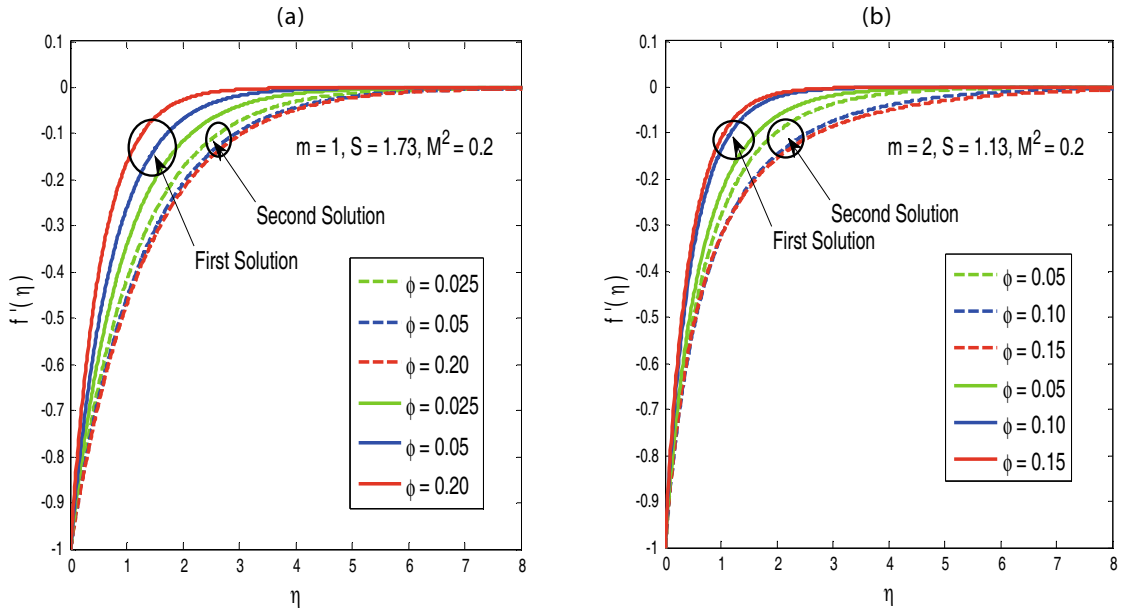

Fig. 7. (a): Variation of velocity profile $f'(\eta)$ for various values of ϕ for $m = 1$. (b): Variation of velocity profile $f'(\eta)$ for various values of ϕ when $m = 2$.

As concerns the velocity profile, it can be observed that both the first and second solutions behave oppositely (see fig. 6(a) and (b)). Obviously the first solution is increasing against the velocity profile $f'(\eta)$ but the boundary layer thickness is decreasing gradually. On the other hand, the behavior of the second solution is different when it is compared with the first solution. Figure 7 depicted the behavior of the velocity profile for the nanoparticle volume fraction ϕ. It is obvious that when the nanoparticles are incorporated in the base fluid (water), the density of the working fluid will slightly increase. Under this observation, the momentum of the nanofluid molecules will be less as compared to the base fluid (water). Consequences of these effects can be observed through fig. 7(a) and (b) while the influence of the suction/injection parameter S on the velocity distribution $f'(\eta)$ is plotted in fig. 8. Similar effects of S on $f'(\eta)$ can be observed for ϕ in fig. 7.

The results plotted in fig. 9 and fig. 10 illustrate the variation of the temperature profile $\theta(\eta)$ against the flow control parameter M and the nanoparticle volume fraction ϕ, respectively. Although the effects of the Hartmann number M on the temperature profile $\theta(\eta)$ seem insignif-

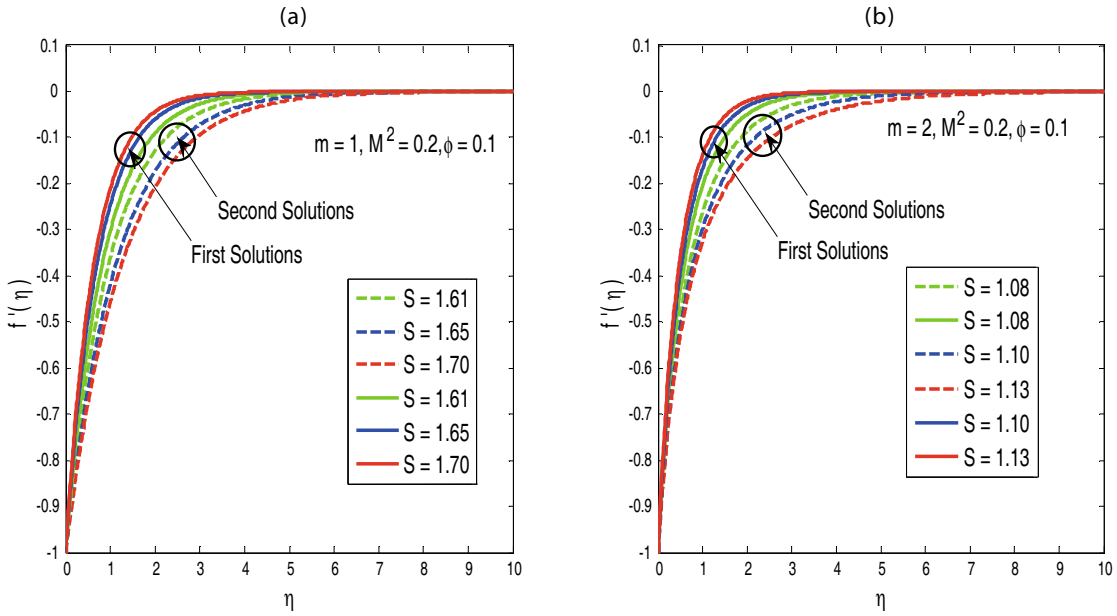

Fig. 8. (a): Variation of velocity profile $f'(\eta)$ for various values of S for $m = 1$. (b): Variation of velocity profile $f'(\eta)$ for various values of S when $m = 2$.

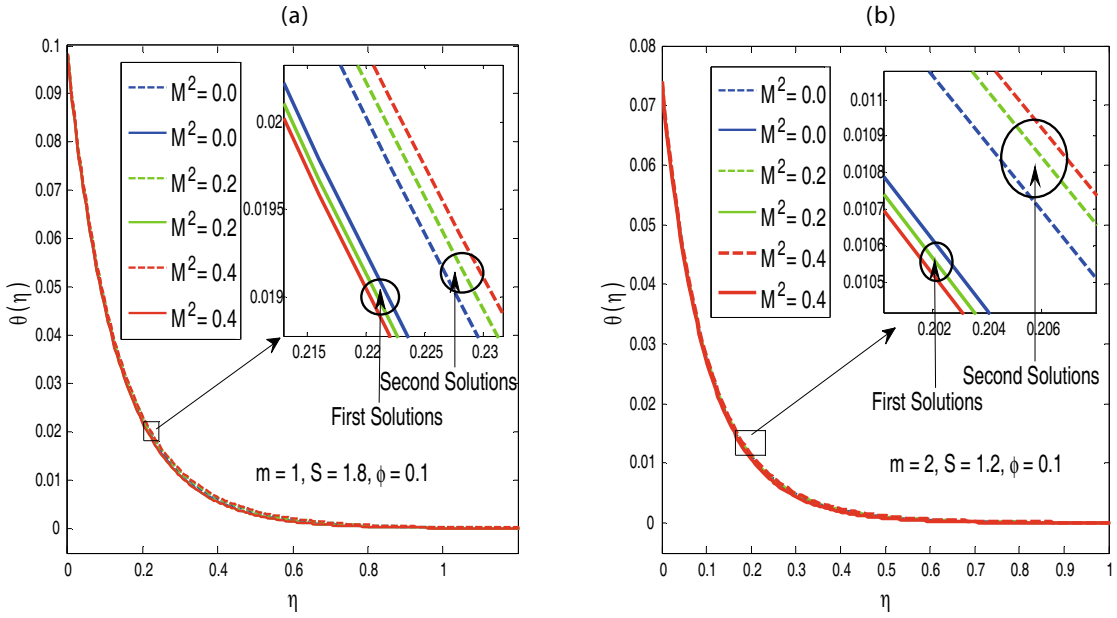

Fig. 9. (a): Variation of temperature profile $\theta(\eta)$ for various values of M for $m = 1$. (b): Variation of temperature profile $\theta(\eta)$ for various values of M when $m = 2$.

icant, if we enlarge the pixels of fig. 9(a) and (b), there is a slight variation in the plots. In both upper and lower branch solutions we can observe that the plotted results have opposite trend with respect to the increasing values of M. Furthermore it is analyzed that when $m = 1$ and $m = 2$, the behaviors in the plotted results are similar, however for the lower solution, the temperature profile decreases whereas in the second solution, the results are comparatively different. According to some experimental studies, it is found that saturation of nanoparticles enhances the thermal conductivity of the working fluid. Similarly, the results plotted in fig. 10 show that an increase in the nanoparticle volume fraction ϕ provides an increase in the temperature. It is found that both unidirectional ($m = 1$) and axisymmetric flow ($m = 2$) have the same effect on the velocity profile.

4.4 Analysis of stream lines and isotherms

Throughout the analysis, although the behaviors of the stream lines and isotherms seem to be the same, slight

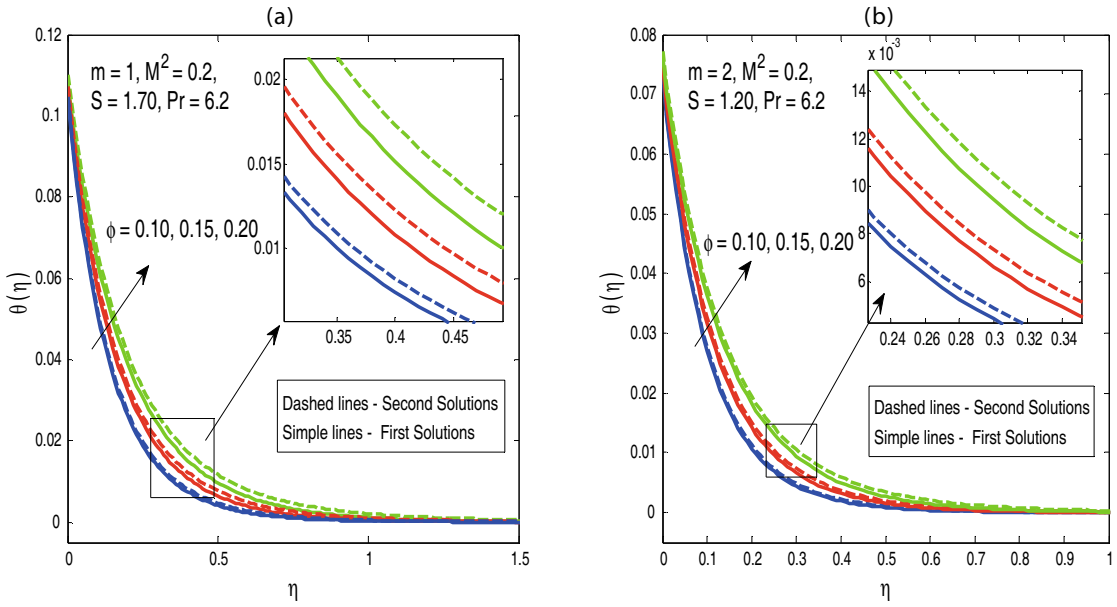

Fig. 10. (a): Variation of temperature profile $\theta(\eta)$ for various values of ϕ for $m = 1$. (b): Variation of temperature profile $\theta(\eta)$ for various values of ϕ when $m = 2$.

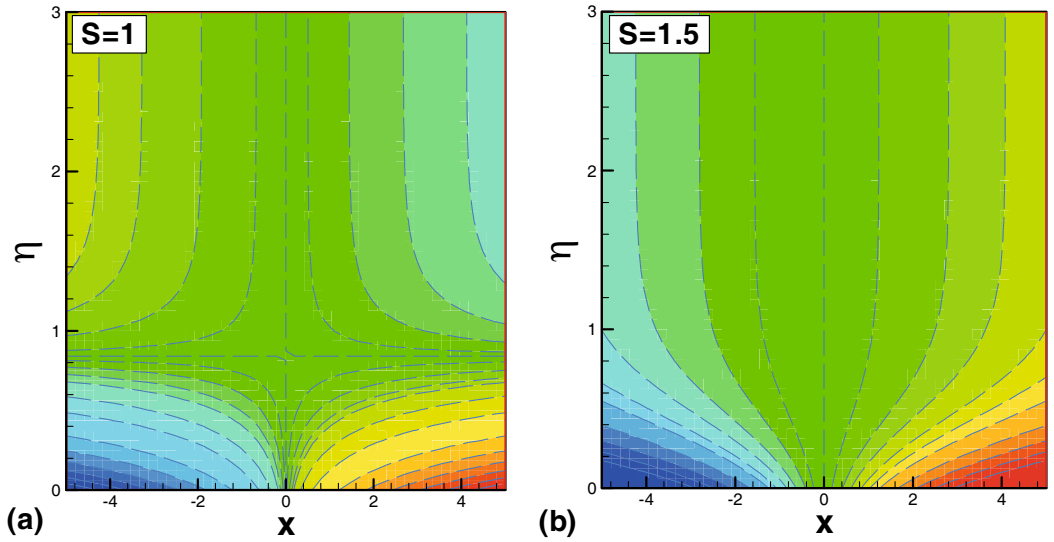

Fig. 11. Variation of stream lines for (a) $S = 1$ and (b) $S = 1.5$.

variations can still be observed as per the suction parameter S and m when the rest of the parameters' values are fixed. To analyze the fluid flow behavior, a family of curves that is instantaneously tangent to the velocity vector of the flow is plotted for the stream function when S varies (see fig. 11). As one can see in fig. 11(a) for $S = 1$ at $x = 0$, the fluid has a stagnation position at about $\eta \approx 0.8$. However for a large value of the suction parameter S, the flow has a continuous streamlines behavior. When the isotherms are drawn with respect to m, one can see that, as $m = 1$, a slightly higher heat transfer at the surface is detected as compared to the case when $m = 2$ (see fig. 12). We further plotted the three-dimensional isotherms behavior in fig. 13 for the suction parameter S and m. It can be observed that with an increase in S or m, the isotherms will gradually decrease.

5 Conclusion

Throughout the analysis, water-based copper nanoparticles are analysed in the presence of a constant magnetic field. Flow distribution is studied at the shrinking surface and to reduce the vorticity effects we have considered a

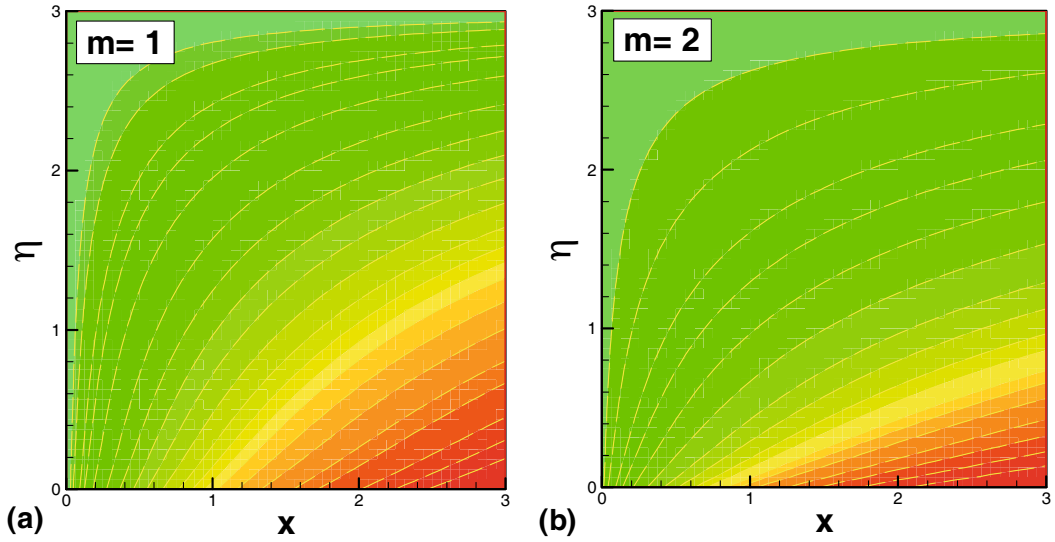

Fig. 12. Variation of isotherms for (a) $m = 1$ and (b) $m = 2$.

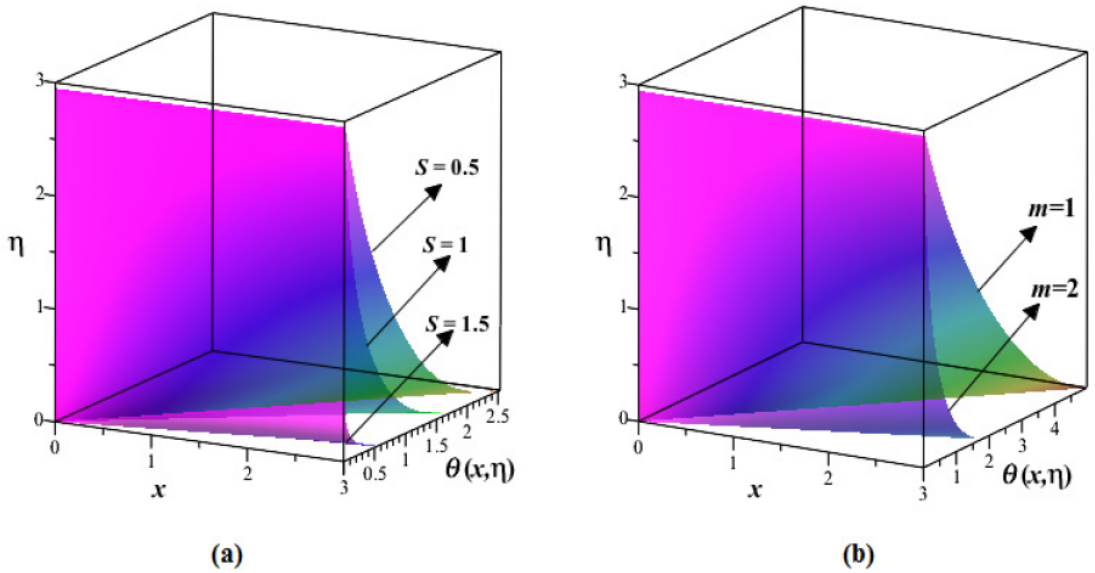

Fig. 13. 3D variation of isotherms for various values of (a) S and (b) m.

permeable surface with suction/injection effects. Results are constructed for both unidirectional ($m = 1$) and axisymmetric ($m = 2$) cases. The range of suction parameters where the dual similar solution exists for increasing values of both Hartmann number and nanoparticle volume fraction are provided in table 2. It is found that the increase in the nanoparticle volume fraction tends to decrease in the velocity profile and raise the skin friction with the sheet. On the other hand, it is further analysed that after saturating the nanoparticle volume fraction, there is a rapid increase in the temperature profile and similarly at the surface of the sheet (Nusselt number). Apart from the nanoparticle volume fraction, other emerging parameters such as the suction parameter S and the Hartmann number M also have a dominant contribution in the increasing behavior of the skin friction and Nusselt number for both upper and lower branch of the solution. Flow behavior and temperature distribution in the whole domain are analyzed through the stream line and isotherms behavior.

The financial support of C.S.I.R., India with appointment of Dinesh Rajotia (one of the authors) as Senior Research Fellowship (SRF) under research scheme no. 09/149(0593)/2011-EMR-I is highly acknowledged.

References

1. S.U.S. Choi, *Enhancing thermal conductivity of fluids with nanoparticles*, in *International Mechanical Engineering Congress and Exposition*, *San Francisco, USA, ASME, FED 231/MD*, Vol. **66** (1995) pp. 99–105.
2. L. Cheng, Recent Patents Engin. **3**, 1 (2009).
3. J. Buongiorno, ASME J. Heat Transfer **128**, 240 (2006).
4. M. Miklavcic, C.Y. Wang, Q. Appl. Math. **64**, 283 (2006).
5. C.Y. Wang, Int. J. Nonlinear Mech. **43**, 377 (2008).
6. Y.Y. Lok, A. Ishak, I. Pop, Int. J. Numer. Methods Heat Fluid Flow **21**, 61 (2011).
7. K. Bhattacharyya, S. Mukhopadhyay, G.C. Layek, Int. J. Heat Mass Transfer **54**, 302 (2011).
8. K. Bhattacharyya, Int. Commun. Heat Mass Transfer **38**, 917 (2011).
9. N.C. Rosca, T. Grason, I. Pop, Sains Malaysiana **41**, 1271 (2012).
10. D.A. Nield, A.V. Kuznetsov, Int. J. Heat Mass Transfer **52**, 5792 (2009).
11. A.V. Kuznetsov, D.A. Nield, Int. J. Thermal Sci. **50**, 712 (2011).
12. W.A. Khan, I. Pop, Int. J. Heat Mass Transfer **53**, 2477 (2010).
13. N. Bachok, A. Ishak, I. Pop, Int. J. Heat Mass Transfer **55**, 2101 (2012).
14. A.M. Rohni, S. Ahmad, A.I. Ismail, I. Pop, Int. Commun. Heat Mass Transfer **43**, 75 (2013).
15. S.K. Nandy, T.R. Mahapatra, Int. J. Heat Mass Transfer **64**, 1091 (2013).
16. Rizwan Ul Haq, Zakia Hammouch, Waqar Ahmed Khan, *Thermal Science*, DOI:10.2298/TSCI141102148H (2015).
17. N.F.M. Noor, Rizwan Ul Haq, S. Nadeem, I. Hashim, Meccanica **50**, 2007 (2015).
18. Wubshet Ibrahim, Rizwan Ul Haq, *J. Brazil. Soc. Mech. Sci. Engin.*, DOI:10.1007/s40430-015-0347-z (2015).
19. W.A. Khan, Z.H. Khan, Rizwan Ul Haq, Eur. Phys. J. Plus **130**, 86 (2015).
20. Rizwan Ul Haq, S. Nadeem, Z.H. Khan, N.F.M. Noor, Physica E **73**, 45 (2015).
21. B.K. Dutta, P. Roy, A.S. Gupta, Int. Commun. Heat Mass Transfer **12**, 89 (1985).
22. T. Ray Mahapatra, A.S. Gupta, Heat Mass Transfer **38**, 517 (2002).
23. N.F.M. Noor, S.A. Kechil, I. Hashim, Commun. Nonlinear Sci. Numer. Simulat. **15**, 144 (2010).